applied sciences

MDPI

Article

Quantitative Analysis of Different Multi-Wavelength PPG Devices and Methods for Noninvasive In-Vivo Estimation of Glycated Hemoglobin

Shifat Hossain, Chowdhury Azimul Haque and Ki-Doo Kim *

Department of Electronics Engineering, Kookmin University, Seoul 02707, Korea; shifathosn@kookmin.ac.kr (S.H.); c_azimul@kookmin.ac.kr (C.A.H.)
* Corresponding author: kdk@kookmin.ac.kr

Abstract: Diabetes is a serious disease affecting the insulin cycle in the human body. Thus, monitoring blood glucose levels and the diagnosis of diabetes in the early stages is very important. Noninvasive in vivo diabetes-diagnosis procedures are very new and require thorough studies to be error-resistant and user-friendly. In this study, we compare two noninvasive procedures (two-wavelength- and three-wavelength-based methods) to estimate glycated hemoglobin (HbA1c) levels in different scenarios and evaluate them with error level calculations. The three-wavelength method, which has more model parameters, results in a more accurate estimation of HbA1c even when the blood oxygenation (SpO_2) values change. The HbA1c-estimation error range of the two-wavelength model, due to change in SpO_2, is found to be from −1.306% to 0.047%. On the other hand, the HbA1c estimation error for the three-wavelength model is found to be in the magnitude of 10^{-14}% and independent of SpO_2. The approximation of SpO_2 from the two-wavelength model produces a lower error for the molar concentration based technique (−4% to −1.9% at 70% to 100% of reference SpO_2) as compared to the molar absorption coefficient based technique. Additionally, the two-wavelength model is less susceptible to sensor noise levels (max SD of %error, 0.142%), as compared to the three-wavelength model (max SD of %error, 0.317%). Despite having a higher susceptibility to sensor noise, the three-wavelength model can estimate HbA1c values more accurately; this is because it takes the major components of blood into account and thus becomes a more realistic model.

Keywords: glycated hemoglobin; error analysis; sensors; mathematical models; photoplethysmography

Citation: Hossain, S.; Haque, C.A.; Kim, K.-D. Quantitative Analysis of Different Multi-Wavelength PPG Devices and Methods for Noninvasive In-Vivo Estimation of Glycated Hemoglobin. *Appl. Sci.* **2021**, *11*, 6867. https://doi.org/10.3390/app11156867

Academic Editors: Alberto Belli, Paola Pierleoni and Sara Raggiunto

Received: 29 June 2021
Accepted: 25 July 2021
Published: 26 July 2021

1. Introduction

Photoplethysmography (PPG) is an optical method of obtaining changes in blood volume in tissue. In the general approach of obtaining PPG signals, the tissue in the region of the digital or radial artery is illuminated with light of multiple wavelengths. The light waves interact with the tissues and blood components and are absorbed or scattered in the medium. As the blood volume changes in a certain location of the human body, due to the pulsatile nature of blood flow, the received light intensity also changes with the change in blood volume.

Historically, PPG signals have been utilized to detect time-domain properties and quantitative properties of the human body. The time-domain properties include—but are not limited to—respiratory rate [1] and heart rate [2]. The most widely used quantitative property of the human body that is measured with PPG signals is the blood oxygenation (SpO_2) parameter [3–5]. This parameter indicates the percent amount of oxygenated hemoglobin with respect to total hemoglobin count. Recently, a study was conducted to warn for potential infection by COVID-19 by estimating SpO_2 using PPG signals [3]. The other quantitative properties include blood pressure [4], hypo- and hypervolemia [5], and

blood glucose levels [6,7]. The time-domain properties require single-wavelength PPG (SW-PPG) to evaluate. On the other hand, to estimate the quantitative properties, multiple wavelengths of PPG (MW-PPG) signals are required.

Diabetes mellitus is a disease that affects the production and utilization of insulin, which directly modifies the consumption of blood glucose by body cells. A result of diabetes is the presence of an excessive amount of glucose available in the bloodstream. This not only changes the properties of the blood but also causes other serious diseases, including kidney failure [8], heart disease [9], and sudden mortality [10]. For these reasons, the diagnosis of diabetes is very important for reducing the risk of insulin control failure in its early stages. There are several methods available to diagnose diabetes. The main approaches for diagnosis are random, fasting, or oral glucose tests, and glycated hemoglobin test.

Estimating blood glucose levels non-invasively for the diagnosis of diabetes is a fairly new topic within the scope of PPG signals [6]. The current state-of-the-art for non-invasive blood glucose estimation is the utilization of external skin tissues and saliva or tears [11,12]. There are also other non-invasive procedures, with which glucose levels can be estimated [13–16].

However, the non-invasive glycated hemoglobin (HbA1c) test is the most recent topic of discussion. Since the invasive test of HbA1c requires blood samples, it can be inconvenient for users to perform tests frequently. HbA1c is the non-enzymatic bond of hemoglobin with sugar molecules. The sugar molecules are usually monosaccharides. The more sugar molecules present in the bloodstream of a person, the more the probability of the glycation of hemoglobin increases. Moreover, the final product of glycation (HbA1c) is very stable and does not usually alter within the life cycle of the glycated hemoglobin molecule. Due to these factors, the HbA1c level in a human body is a very slow varying parameter, and is usually considered equivalent to the three-month weighted average of the blood sugar level [17]. Measurement of hyperglycemia-associated conditions was performed on mice models to classify normal, obese, and diabetic groups in a recent study [18]. In another study, the researchers designed a method to estimate HbA1c by measuring breath acetone components [19]. There are only two papers that conducted studies on the estimation of glycated hemoglobin using PPG signals. One of the studies performed an in vitro analysis from the blood sample [20], and the other study was designed to measure the HbA1c by in vivo measurement [21].

Although PPG signals are characterized as an easy-to-acquire optical signal compared to other bodily signals (e.g., EEG (Electroencephalography), ECG (Electrocardiography), ABP (Arterial Blood Pressure)), there are specific methods and wavelength selection procedures that are required to obtain a good quality signal.

Among the wavelength-dependent methods, SW-PPG, MW-PPG, and all-wavelength PPG (AW-PPG) are employed based on the purpose of the signal acquisition. As described previously, time-dependent properties usually require SW-PPG. On the other hand, MW-PPG and AW-PPG are employed in the measurement of quantitative properties. Since glycated hemoglobin is a quantitative property of blood, an MW-PPG or AW-PPG signal is required for estimation.

The most widely used technique for acquiring an MW-PPG signal uses discrete LEDs of different wavelengths and single or multiple photodetectors (PDs) to record the PPG signals. In this method, the specimen or medium is placed between the LEDs and PDs for transmission-mode PPG, and the medium is placed on one side of the LED-PD arrangement for reflection-mode PPG signal acquisition. In the reflection mode PPG system, the LEDs and PDs are placed in a single plane facing at the medium. Figure 1 depicts the different arrangements of LEDs and PDs for PPG signal acquisition.

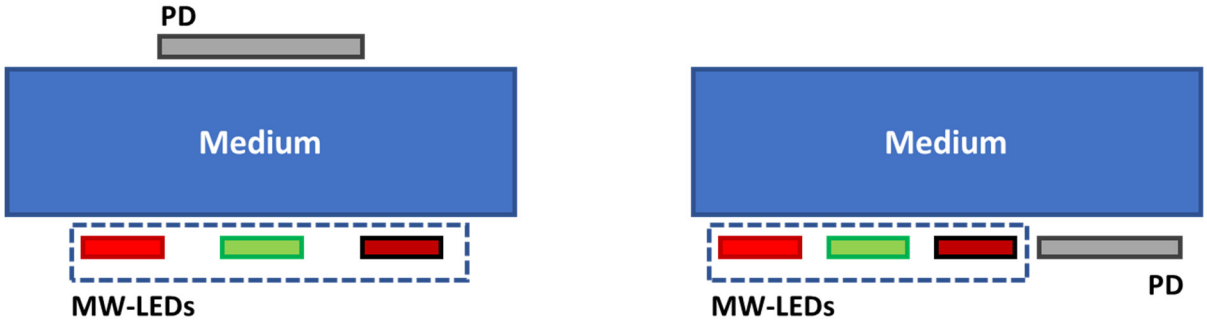

Figure 1. Discrete-LED/PD-based transmission- (left) and reflection-mode (right) PPG acquisition devices.

The advent of wearable and mobile devices has led to an exponential increase in mobile-based healthcare systems. Smartphones with powerful processors, multiple sensors, and large data storage capabilities are well suited for healthcare systems. A smartphone camera can be a great candidate for a PPG signal acquisition device, where the camera sensor is the PD and the white built-in flashlight is the light source. In this case, the light source contains a wide range of wavelengths interacting with the medium, and the camera sensor filters the input light into three distinct wavelengths (red, green, and blue). The different signals from these three wavelengths can be utilized as an MW-PPG signal. Transmission- and reflection-mode PPG signals can also be acquired using smartphone cameras by placing the white LED on the opposite side of the medium or at the same plane of the camera sensor, respectively. Figure 2 illustrates the different modes of PPG signal for a camera-sensor-based PPG system.

Figure 2. Camera-sensor white-LED MW-PPG system. The left figure is the transmission mode and the right figure is the reflection mode.

In this study, we compare the camera-sensor-based and discrete-LED/PD-based processes of MW-PPG acquisition to estimate in vivo glycated hemoglobin. We also perform comparative analyses on the two PPG-based HbA1c estimation methods described in [20]. In this manuscript, the study of [17] is described as a two-wavelength based method, and the study of [18] is described as a three-wavelength based method for estimating glycated hemoglobin.

2. Methodology

In a recent study [21], we built a finger model based on the hypothesis that when blood enters a tissue the total volume of the tissue expands, increasing the amount of light traversing a path through the tissue medium.

Moreover, the study also hypothesized that the blood constitutes oxyhemoglobin (HbO), deoxyhemoglobin (HHb), and glycated hemoglobin (HbA1c). The HbA1c component of blood is stated to be fixed at a mixture of 98% oxygenated and 2% deoxygenated HbA1c. So, the total absorption coefficient of the blood solution becomes

$$C_a = \epsilon_a^{\mathrm{HbA1c}}(\lambda) \times c_{\mathrm{HbA1c}} + \epsilon_a^{\mathrm{HbO}}(\lambda) \times c_{\mathrm{HbO}} + \epsilon_a^{\mathrm{HHb}}(\lambda) \times c_{\mathrm{HHb}} \quad (1)$$

$$C_a = \mu_a^{\mathrm{HbA1c}}(\lambda) + \mu_a^{\mathrm{HbO}}(\lambda) + \mu_a^{\mathrm{HHb}}(\lambda) \quad (2)$$

In (1) and (2), C_a, ϵ, and c are the total absorption coefficient of the blood solution, molar absorption coefficient, and molar concentration of the individual component of the solution, respectively.

From another study [20], we can obtain a different blood-solution hypothesis to estimate the amount of glycated hemoglobin in the blood. According to the hypothesis, the blood solution only contains glycated and non-glycated hemoglobin components. So, the blood solution absorption coefficient expression becomes

$$C_a = \epsilon_a^{\mathrm{HbA1c}} c_{\mathrm{HbA1c}} + \epsilon_a^{\mathrm{NonHbA1c}} c_{\mathrm{NonHbA1c}} \quad (3)$$

$$C_a = \mu_a^{\mathrm{HbA1c}} + \mu_a^{\mathrm{NonHbA1c}} \quad (4)$$

The system from (3) and (4) greatly simplifies the actual finger structure. The non-HbA1c component of (3) and (4) mostly indicates the homogenous mixture of 98% oxyhemoglobin and 2% deoxyhemoglobin compounds. So,

$$\epsilon_a^{\mathrm{NonHbA1c}} = \epsilon_a^{\mathrm{HbO}} \times 0.98 + \epsilon_a^{\mathrm{HHb}} \times 0.02 \quad (5)$$

Now, from the Beer–Lambert law

$$A = C_a d = -\log\left(\frac{I}{I_0}\right) \quad (6)$$

In (6), A, d, I, and I_0 denote the total solution absorbance, light transmission path length, received light, and the incident light, respectively. Applying (6) in (1) and (3) with different wavelengths of light can enable us to calculate the parameters of (1) and (3), respectively.

Now, placing (1) in (6), we get

$$A(\lambda) = \left(\epsilon_a^{\mathrm{HbA1c}}(\lambda) \times c_{\mathrm{HbA1c}} + \epsilon_a^{\mathrm{HbO}}(\lambda) \times c_{\mathrm{HbO}} + \epsilon_a^{\mathrm{HHb}}(\lambda) \times c_{\mathrm{HHb}}\right) d = -\log\left(\frac{I(\lambda)}{I_0(\lambda)}\right) \quad (7)$$

Similarly, placing (3) in (6), we get

$$A(\lambda) = \left(\epsilon_a^{\mathrm{HbA1c}} c_{\mathrm{HbA1c}} + \epsilon_a^{\mathrm{NonHbA1c}} c_{\mathrm{NonHbA1c}}\right) d = -\log\left(\frac{I(\lambda)}{I_0(\lambda)}\right) \quad (8)$$

From the discussion of these models, it can be deduced that the oxyhemoglobin and deoxyhemoglobin are kept fixed in the latter model, which may lead to more errors due to the change of blood oxygenation level (SpO_2) in the bloodstream. The processes of error analysis are described in the following subsections.

A. Error analysis between HbA1c estimation models

To analyze the error level of the models, a reference model should be set. As the first model (7) consists of most of the blood parameters (i.e., oxy-, deoxy-, and glycated hemoglobin), it is considered to be the reference model for estimating the error of the second model due to change in SpO_2 levels.

Now, to estimate the error level of the second model, the models are analyzed within a range of HbA1c and SpO_2 levels. The HbA1c range is set to 4–14%, and the SpO_2 is set to 70–100%. For each value of HbA1c and SpO_2, the c_{HbA1c}, c_{HbO}, and c_{HHb} parameters

are calculated using the following equations and placed in (7) to calculate absorbance values for a certain wavelength.

$$c_{\mathrm{HbA1c}} = \frac{\%\mathrm{HbA1c}}{100} \times c_{\mathrm{Wb}} \tag{9}$$

$$c_{\mathrm{HbO}} = \left(1 - \frac{\%\mathrm{HbA1c}}{100}\right) \times \frac{\%\mathrm{SpO_2}}{100} \times c_{\mathrm{Wb}} \tag{10}$$

$$c_{\mathrm{HHb}} = \left(1 - \frac{\%\mathrm{HbA1c}}{100}\right) \times \left(1 - \frac{\%\mathrm{SpO_2}}{100}\right) \times c_{\mathrm{Wb}} \tag{11}$$

$$c_{Wb} = 2.2\ \mathrm{mol\ L^{-1}} = 2.2 \times 10^{-3}\mathrm{M} \tag{12}$$

Now from (7), we can define the terms %HbA1c and %SpO_2 as

$$\%\mathrm{HbA1c} = \frac{c_{\mathrm{HbA1c}}}{c_{\mathrm{HbA1c}} + c_{\mathrm{HbO}} + c_{\mathrm{HHb}}} \times 100\% \tag{13}$$

$$\%\mathrm{SpO_2} = \frac{c_{\mathrm{HbO}}}{c_{\mathrm{HbO}} + c_{\mathrm{HHb}}} \times 100\% \tag{14}$$

In (9)–(12), the term c_{Wb} indicates the molar concentration of whole blood.

After calculating the c_{HbA1c}, c_{HbO}, and c_{HHb} parameters for a set of HbA1c and SpO_2 values, these are placed in (7) to calculate the absorbance values $A(\lambda_1)$, $A(\lambda_2)$, and $A(\lambda_3)$ for three wavelengths—λ_1, λ_2, and λ_3—respectively, considering the value of d as 1 cm. These three absorbance values are then used to reversely calculate the c_{HbA1c}, c_{HbO}, and c_{HHb} parameters from (7) and c_{HbA1c} and c_{NonHbA1c} parameters from (8), using the least square curve fitting algorithm. Due to the differences between the model approximations, the reversely calculated parameters will be different and will result in errors.

B. SpO_2 approximation error from model (8)

Though the c_{HbO} and c_{HHb} parameters cannot be directly evaluated from (8) to estimate the SpO_2 value, these parameters can be approximated with certain considerations.

For the first consideration from (8), the c_{NonHbA1c} parameter can be hypothesized as being very close to c_{HbO}, as the c_{NonHbA1c} contains 98% of the c_{HbO} parameter. So,

$$c_{\mathrm{NonHbA1c}} \approx c_{\mathrm{HbO}} \tag{15}$$

Thus, from (9) and (10), we can state that,

$$c_{HbO} = \frac{\%\mathrm{SpO_2}}{100} \times c_{\mathrm{Wb}} - c_{\mathrm{HbA1c}} \times \frac{\%\mathrm{SpO_2}}{100}$$

$$\%\mathrm{SpO_2} = \frac{c_{\mathrm{HbO}}}{c_{\mathrm{Wb}} - c_{\mathrm{HbA1c}}} \times 100 \tag{16}$$

Now, from (15) and (16) we determine the molar concentration based approximation as below.

$$\%\mathrm{SpO_2} \approx \frac{c_{\mathrm{NonHbA1c}}}{c_{\mathrm{Wb}} - c_{\mathrm{HbA1c}}} \times 100 \tag{17}$$

On the other hand, $\epsilon_a^{\mathrm{NonHbA1c}}$ can be considered as a mixture of ϵ_{HbO} and ϵ_{HHb}, corresponding to the blood oxygenation level.

$$\epsilon_a^{\mathrm{NonHbA1c}} = \epsilon_a^{\mathrm{HbO}} \times \frac{\%\mathrm{SpO_2}}{100} + \epsilon_a^{\mathrm{HHb}} \times \left(1 - \frac{\%\mathrm{SpO_2}}{100}\right) \tag{18}$$

Now, from (8) it can be said that,

$$\frac{A - c_{\mathrm{HbA1c}}\epsilon_a^{\mathrm{HbA1c}} d}{d\, c_{\mathrm{NonHbA1c}}} = \epsilon_a^{\mathrm{NonHbA1c}}$$

$$\frac{A - c_{\mathrm{HbA1c}}\epsilon_a^{\mathrm{HbA1c}} d}{d\, c_{\mathrm{NonHbA1c}}} = \epsilon_a^{\mathrm{HbO}} \times \frac{\%\mathrm{SpO}_2}{100} + \epsilon_a^{\mathrm{HHb}} \times \left(1 - \frac{\%\mathrm{SpO}_2}{100}\right)$$

So, the molar absorption coefficient based approximation becomes

$$\%\mathrm{SpO}_2 = \frac{\frac{A - c_{\mathrm{HbA1c}}\epsilon_a^{\mathrm{HbA1c}} d}{d\, c_{\mathrm{NonHbA1c}}} - \epsilon_a^{\mathrm{HHb}}}{\epsilon_a^{\mathrm{HbO}} - \epsilon_a^{\mathrm{HHb}}} \times 100 \tag{19}$$

Using (17) and (19), SpO_2 values can be approximated for the second model of (8).

C. Model error due to sensor-induced noise levels

The PDs used in discrete-LED/PD systems and the color sensor used in the camera-sensor-based PPG signal acquisition system have their own sensitivity, noise level, sampling rate, and quantization limitations. In this study, we perform a noise analysis on the models (7) and (8), which is based on the experimental noise levels obtained from two different sensors. The noise is added to the received light intensity of the sensor and the c_{HbA1c}, c_{HbO}, and c_{HHb} parameters are reversely calculated using the least square curve fitting method.

To estimate the estimation error due to sensor-induced noise, the HbA1c and SpO_2 levels are taken in a range as previously described. Utilizing (9) to (12), different parameters are evaluated and placed in (7) to calculate the absorbance values $A(\lambda_1)$, $A(\lambda_2)$, and $A(\lambda_3)$ in different wavelengths of light. Two ratio values are also calculated from these absorbance values to cancel out the light traversing path length term, d. From the original hypothesis of [21], we can say that the parameter d will change slightly when the blood enters a tissue region. So,

$$\delta d = d_1 - d_2 \text{ and } \delta A(\lambda) = A_1(\lambda) - A_2(\lambda)$$

Here, A_1 and A_2 indicate the two absorbance values at d_1 and d_2, respectively. These two values, d_1 and d_2, represent the diameter of the blood vessel when blood enters and leaves the vessel, respectively. So, we can define the ratio terms from these equations as (20) and (21).

$$R_1 = \frac{\delta A(\lambda_1)}{\delta A(\lambda_3)} = \frac{\left[log\frac{I(d_2)}{I(d_1)}\right]_{\lambda 1}}{\left[log\frac{I(d_2)}{I(d_1)}\right]_{\lambda 3}} \tag{20}$$

$$R_2 = \frac{\delta A(\lambda_2)}{\delta A(\lambda_3)} = \frac{\left[log\frac{I(d_2)}{I(d_1)}\right]_{\lambda 2}}{\left[log\frac{I(d_2)}{I(d_1)}\right]_{\lambda 3}} \tag{21}$$

At this stage, the received light values are calculated from (6), and a noise parameter is added with the received light for each set of HbA1c and SpO_2 values,

$$I(\lambda) = I_0 10^{-A} \tag{22}$$

$$I'(\lambda) = I(\lambda) + N \tag{23}$$

In (23), $I'(\lambda)$ is the noisy received light when a Gaussian noise N is added with the ideal received light, $I(\lambda)$. The values of the terms d_1 and d_2 cancel out in the ratio equations.

After adding noise to the received light, the ratio values are calculated using (20) and (21), resulting in R_1' and R_2'. These two ratio values are used to inversely calculate the c_{HbA1c}, c_{HbO}, and c_{HHb} parameters from (7) and c_{HbA1c} and c_{NonHbA1c} parameters from (8), respectively, using the least square curve fitting algorithm. We then calculate the HbA1c estimation error for different models in different sensor-induced noise levels.

3. Results

To quantitatively analyze the errors associated with the analysis methods described in the previous section, we have selected 3 wavelengths of light ($\lambda_1 = 465$ nm, $\lambda_2 = 525$ nm, and $\lambda_3 = 615$ nm). The molar absorption coefficients for these selected wavelengths are given in Table 1.

Table 1. Table of molar absorption coefficients of HbA1c [22], HbO, and HHb [23] for selected wavelengths.

Wavelength (nm)	HbA1c ($\mathbf{M^{-1}cm^{-1}}$)	HbO ($\mathbf{M^{-1}cm^{-1}}$)	HHb ($\mathbf{M^{-1}cm^{-1}}$)
465	549,024.7353	38,440.2	18,701.6
525	455,139.5677	30,882.8	35,170.8
615	170,555.4218	1166.4	7553.4

A. Error analysis between HbA1c estimation models

Comparing model (7) with the model (8) by the process described in the previous section, taking (7) as a reference, yields two error metrics: HbA1c error and SpO_2 error. Figure 3 illustrates the HbA1c and SpO_2 error for model (7), and the HbA1c error for model (8). The SpO_2 error is not shown in this section as the SpO_2 parameter cannot be directly deduced from the model (8). The SpO_2 approximation results and errors are described in the following sub-section.

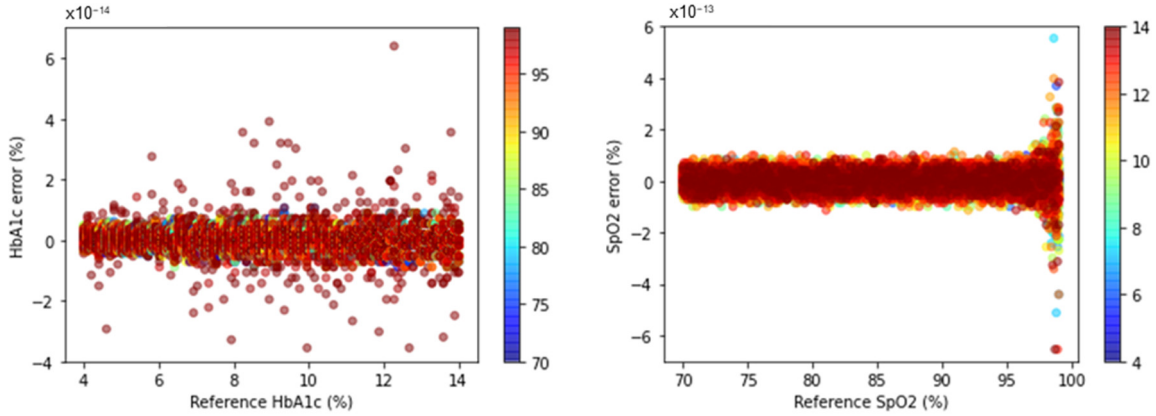

(**a**) (**b**)

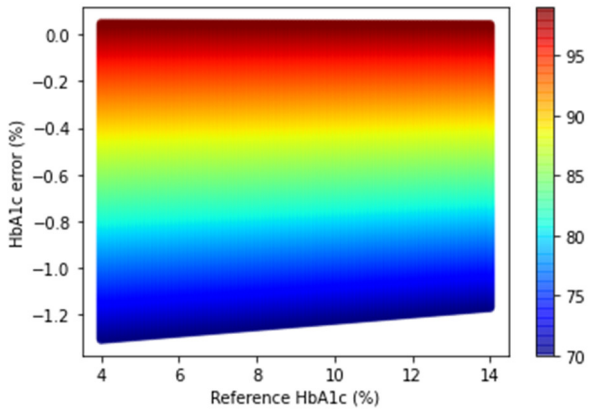

(**c**)

Figure 3. Error analysis between HbA1c estimation models: (**a**) HbA1c error for model (7), (**b**) SpO_2 estimation error for model (7), and (**c**) HbA1c estimation error for model (8). For (**a**,**c**), the color bar represents the reference SpO_2 values and the color bar in (**b**) represents reference HbA1c values.

In Figure 3, the estimation error associated with the model (7) and (8) based systems with respect to reference values is shown. Figure 3a–b illustrate the estimation error of HbA1c and SpO_2 associated with the model (7), whereas Figure 3c depicts the estimation error of HbA1c with the model (8).

The color bars drawn in Figures 3a–c show the corresponding reference SpO_2 level for each data point. The color bar in Figure 3b shows the reference HbA1c value for each estimation data point of SpO2.

In Figures 3a–b, the model-(7)-based HbA1c and SpO_2 estimation error is in the range of 10^{-14} and 10^{-13}, respectively. These error values can be associated with floating-point errors in computing algorithms. In Figure 3c, the HbA1c estimation error varies from -1.306% to 0.047%. This large error is due to the lack of parameters for changes in blood oxygenation level.

The mean of the error levels for Figure 3a,c are found to be 8.52^{-17}, -1.60^{-15}, and −0.60, respectively. The standard deviation (SD) values of the error levels are also found to be 2.90^{-15}, 3.31^{-14}, and 0.37, respectively, for the corresponding plots.

B. SpO_2 approximation error from model (8)

The blood oxygenation parameter can be approximated from the model (8). Two equations, (17) and (19) were derived to approximate the SpO_2 value. Equation (17) only depends on estimated non-HbA1c and HbA1c molar concentrations, whereas (19) depends on light-wavelength-dependent properties. So, approximating SpO_2 with (19) can render different SpO_2 approximations for different wavelengths of light. Figure 4 shows the SpO_2 approximation error for (17).

The molar concentration based SpO_2 approximation results give an error range of −4% to −1.9% in the range of 70 to 100% reference SpO_2 values. Figure 5 depicts the SpO_2 approximation error of (19) for 465 nm, 525 nm, and 615 nm.

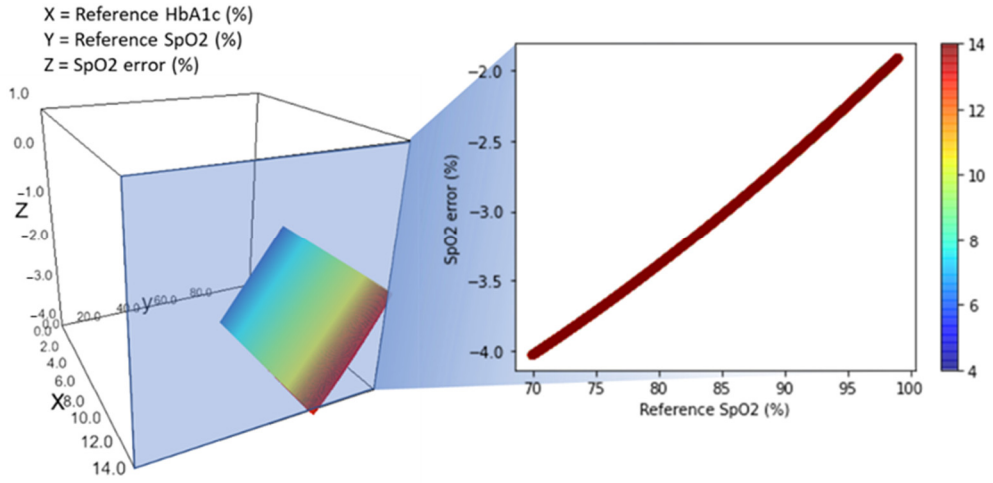

Figure 4. Molar concentration based SpO_2 approximation error for (17) from the model (8).

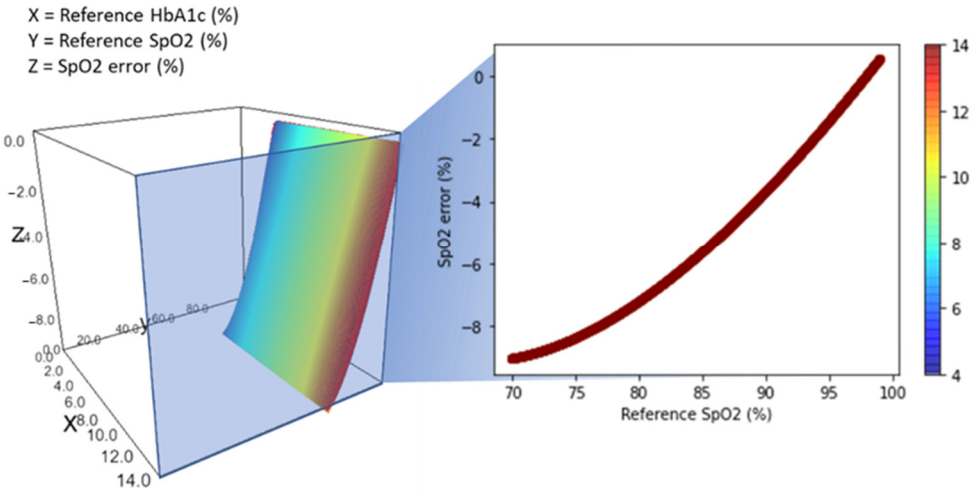

(**a**)

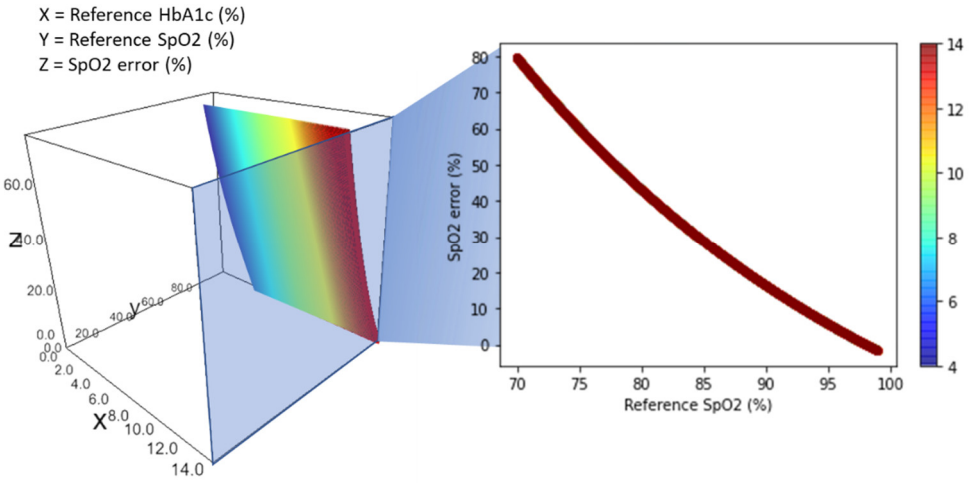

(**b**)

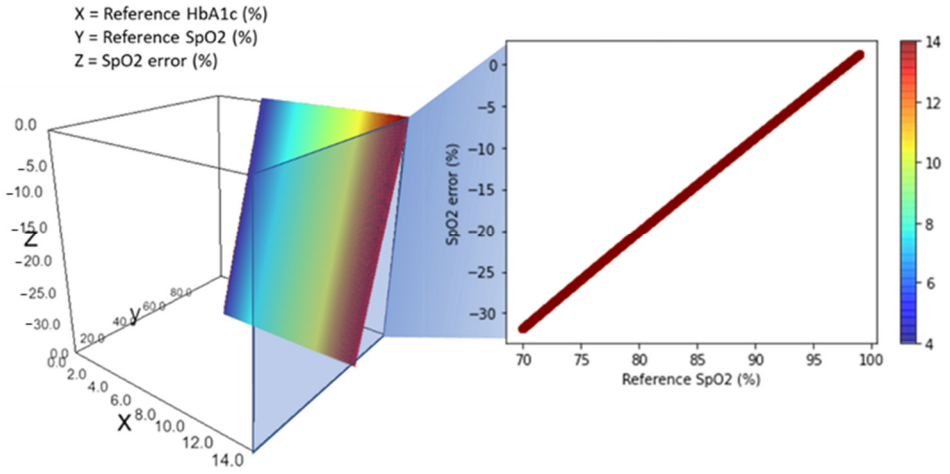

(**c**)

Figure 5. Molar absorption coefficient based SpO_2 approximation error of (19) for (**a**) 465 nm, (**b**) 525 nm, and (**c**) 615 nm. The color bar represents the reference HbA1c values.

The 3-dimensional plots of Figures 4 and 5a, c illustrate the approximation error of SpO_2 using model (8). The X, Y, and Z axes of the plots are reference HbA1c, reference SpO_2, and SpO_2 approximation error, respectively. The 2-dimensional plot beside the 3-dimensional figure depicts the Y-Z plane, which is the SpO_2 approximation error vs. reference SpO_2 values.

From all these figures (Figures 4 and 5), we can see that the SpO_2 values do not depend on the HbA1c values. Furthermore, for the approximation with (19), the error range changes depend upon the wavelength selection. A reduction in the oxygenation of the blood sample increases the approximation error of SpO_2. As a result, the minimum approximation error can be found for 465 nm (−9 at SpO_2 70% and about 1 at SpO_2 100%).

C. Model error due to sensor induced noise levels

To examine the sensor-induced noise levels in the HbA1c estimation models, we considered two sensors for PPG acquisition. One of the sensors is the Osram SFH7050 with AFE4404 and the other is the TCS34725 color sensor. The Osram SFH7050 and AFE4404 pair are considered as a discrete-LED/PD-based PPG acquisition system. On the other hand, the TCS34725 is considered to be a camera-sensor-based PPG acquisition system. According to our tests on these sensors, the standard deviation (SD) of error values generated by the AFE4404 front end is 1.820×10^{-4} for transmission-mode PPG, and 1.480×10^{-4} for reflection mode PPG signals. The TCS34725 sensor has an SD of 3.640×10^{-5} and 6.711×10^{-5} for transmission and reflection mode PPG signals, respectively.

Considering the method described in subsection C of the Methodology section, the width of the Gaussian function is set using the SD values obtained from the different sensors for different modes, as given previously. Figure 6 shows the HbA1c values estimated from the noise-prone ratio values (R_1 and R_2) for the AFE4404 based sensor and PPG mode. On the other hand, Figure 7 illustrates the HbA1c estimation error for the TCS34725 sensor.

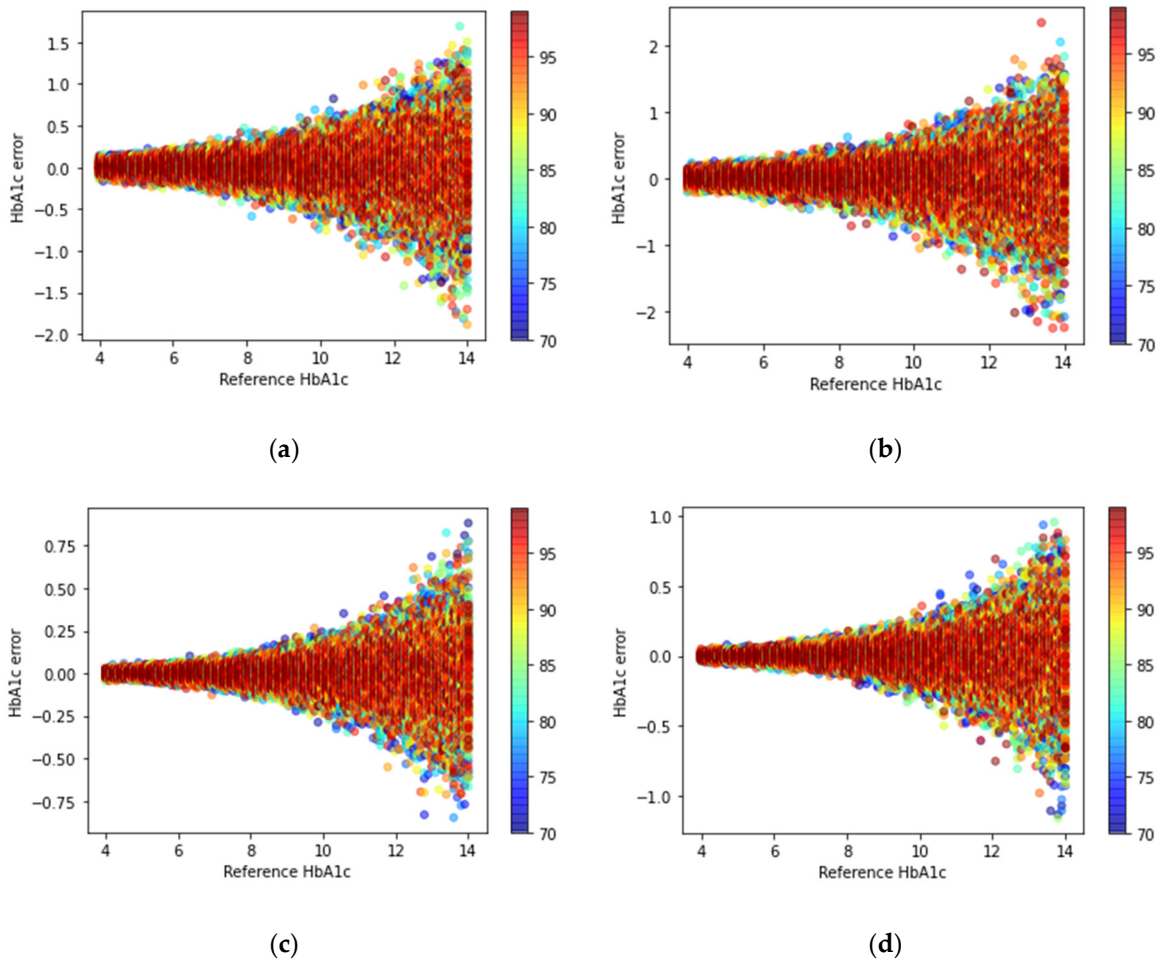

Figure 6. HbA1c estimation error due to AFE4404-based sensor-induced noise. Model-(7)-based HbA1c estimation values are illustrated for (**a**) reflection-mode and (**b**) transmission-mode PPG signal. Model-(8)-based estimation values are given for (**c**) reflection-mode and (**d**) transmission-mode PPG signals. The color bar represents the reference SpO2 values.

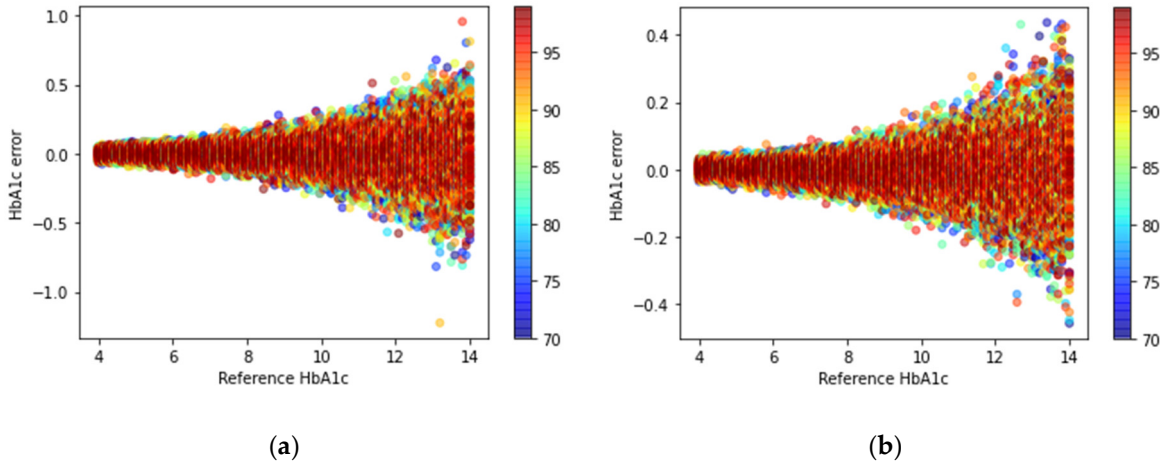

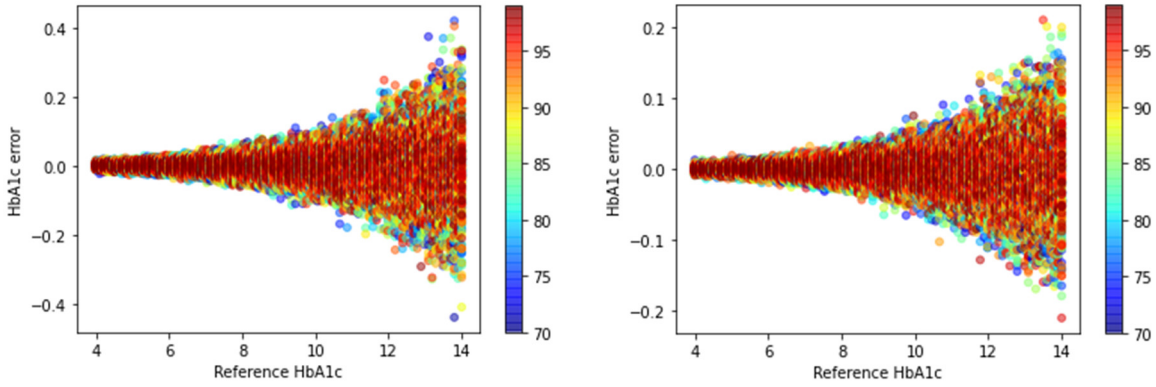

(**c**) (**d**)

Figure 7. HbA1c estimation error due to TCS34725 sensor-induced noise. Model-(7)-based HbA1c estimation values are illustrated for (**a**) reflection-mode and (**b**) transmission-mode PPG signal. Model-(8)-based estimation values are given for (**c**) reflection-mode and (**d**) transmission-mode PPG signals. The color bar represents the reference SpO2 values.

In Figure 6, the estimation error of HbA1c is illustrated with respect to reference HbA1c values for model (7) (Figure 6a–b) and model (8) (Figure 6c–d), respectively. From all these figures it is evident that the estimation error level increases as the HbA1c level increases. This is due to the high light attenuation property of HbA1c molecules. An increment of HbA1c molecules inside a solution can lead to reduced amplitudes in received light signals, resulting in greater errors in estimation.

The standard deviation (SD) of the erroneous estimation for the AFE4404-based sensor of the model (7) is found to be 0.258 and 0.317 for reflection and transmission modes, respectively. On the other hand, model (8) has an SD of 0.114 and 0.142 for reflection and transmission modes, respectively.

Figure 7 also depicts similar illustrations to Figure 6. However, since the TCS34725 sensor receives less signal noise than the AFE4404, the SD of the estimation error of HbA1c is reduced greatly, which can be seen in Figure 7.

The SD of the erroneous estimation of the model (7) is found to be 0.117 and 0.063 for reflection and transmission modes, respectively. For model (8), SD is found to be 0.052 and 0.028, in reflection and transmission modes, respectively.

4. Discussion

From the above discussions that assess the two models for their different errors in estimating in vivo glycated hemoglobin values, certain important points can be made. Upon comparing the two models (model (7) and model (8)), it can be easily seen that model (8) is a simplified version of model (7). Model (8) combines the oxygenated and deoxygenated hemoglobin parts into one variable. For this reason, a change in the blood oxygenation value (i.e., a change in the ratio of oxygenated and deoxygenated hemoglobin count in the bloodstream) can significantly impair the HbA1c estimation accuracy of model (8).

On the contrary, model (7) is more susceptible to the sensor noise, degrading the estimation accuracy of glycated hemoglobin as compared to model (8). This occurs as model (7) is more complex and more parameters are built into the model equation itself. As a result, any error in the input of the model amplifies the error with the model parameters and gives more erroneous results. From Figure 6 and Figure 7, we can see that the error level of model (7) is almost double when compared to the error level of the model (8) for both modes of PPG signal using the AFE4404-based sensor and TCS34725-based sensor. Though the sensitivity of model (7) to noise is large compared to model (8), model (7) can

be made robust against sensor noise by taking multiple sampling processes in the application of the model. The sensors usually exhibit random noise in the signals. Taking the arithmetic mean of several samples of measurement can ensure the reduction of random noise, hence reducing random estimation error.

From Figures 6 and 7, it is also evident that the more the HbA1c components are present in the blood solution, the greater the error level becomes. This is due to the fact that the glycated hemoglobin component of blood has a much higher molar absorption coefficient than that of the other two components of blood considered in this study (HHb and HbO). Thus, an increase in HbA1c decreases the received light intensity, and consequently decreases the signal-to-noise ratio for a fixed amount of added noise, resulting in poor estimation accuracy.

5. Conclusions

In this study, we performed a quantitative analysis on two models for the non-invasive estimation of glycated hemoglobin (HbA1c). Comparing the two models, by taking one as a reference for different parametric states, the two-wavelength model was found to have errors in the range of −1.306% to 0.047% of HbA1c, depending on the amount of oxygenated and deoxygenated hemoglobin compounds present in the blood solution. On the other hand, the three-wavelength model's HbA1c-estimation error was found to have a magnitude of 10^{-14} %.

From the approximation of the blood oxygenation (SpO_2) value of the two-wavelength model, it can be seen that a lower error can be attained by using the molar concentration based SpO_2 approximation technique, as compared to the molar absorption coefficient based method. The method based on the molar absorption coefficient depends on the wavelength of the light and, in our experiment, we observed that the light at a wavelength of 465 nm produced the lowest error for the two-wavelength-based SpO_2 approximation.

Finally, from the estimation error of HbA1c due to sensor noise level, it can be seen that the two-wavelength-based model has a higher resistance to sensor noise, and that the three-wavelength-based model is more susceptible to noise due to the higher complexity of the model. Though the two-wavelength based model has a low error level even when the sensor noise is high, the model performs poorly (error range varies between −1.306% and 0.047% with the change in SpO_2 values) when estimating the glycated hemoglobin as compared to the three-wavelength based model. This is because the two-wavelength based model does not consider the two major hemoglobin components of blood.

Authors' Contributions: S.H.: conceptualization, methodology, software, validation, data curation, visualization. C.A.H.: software, validation, data curation, investigation. K.-D.K.: conceptualization, validation, supervision, formal analysis, funding acquisition. All authors have read and agreed to the published version of the manuscript.

Funding: This research was supported by the Basic Science Research Program through the National Research Foundation (NRF) of Korea, funded by the Ministry of Education (NRF-2019R1F1A1062317), and was also supported by the National Research Foundation of Korea Grant, funded by the Ministry of Science, ICT, and Future Planning [2015R1A5A7037615].

Conflicts of Interest: The authors hereby declare that they have no conflict of interest. The funders had no role in the design of the study; in the collection, analyses, or interpretation of data; in the writing of the manuscript; or in the publication of the results.

Short Biography of Authors

Shifat Hossain was born in Dhaka, Bangladesh, on 10 May 1994. He received a Bachelor of Science (B.Sc.) degree in Electrical and Electronic Engineering from the Khulna University of Engineering and Technology, Bangladesh, in 2017. Later he received his Master of Science (M.Sc.) degree in 2021 from Department of Electronics Engineering, Kookmin University, Seoul, South Korea. He is currently appointed as a full-time researcher in the Department of Electronic Engineering, Kookmin University. He worked as a Lecturer with the Department of Electrical and Electronic Engineering, Daffodil International University from September 2018 to February 2019. His current fields of study are machine learning algorithms and computational biomedical engineering.

Chowdhury Azimul Haque received a Bachelor of Science (B.Sc.) degree in electrical and electronic engineering from Khulna University of Engineering and Technology (KUET), Bangladesh, in 2019. He is currently pursuing a Master of Science (M.Sc.) degree in electronics engineering with Kookmin University, Seoul, Korea. His current research interests include biomedical signal processing and Monte Carlo simulations in computational biomedical engineering.

Ki-Doo Kim received a B.S. degree in Electronic Engineering from Sogang University, Seoul, South Korea, in 1980, and the M.S. and Ph.D. degrees from Pennsylvania State University, USA, in 1988 and 1990, respectively. He is currently working as a Professor with the School of Electrical Engineering, Kookmin University, Seoul. He worked as a Research Engineer with the Agency for Defense Development in Korea from 1980 to 1985. He joined Kookmin University as an Assistant Professor in 1991. He also served as a Visiting Scholar with the EE Department, UCSD, USA, from 1997 to 1998. His current research interests include digital communication and signal processing.

References

1. Chang, H.; Hsu, C.; Chen, C.; Lee, W.; Hsu, H.; Shyu, K.; Yeh, J.; Lin, P.; Lee, P. A Method for Respiration Rate Detection in Wrist PPG Signal Using Holo-Hilbert Spectrum. *IEEE Sens. J.* **2018**, *18*, 7560–7569, doi:10.1109/JSEN.2018.2855974.
2. Temko, A. Accurate Heart Rate Monitoring During Physical Exercises Using PPG. *IEEE Trans. Biomed. Eng.* **2017**, *64*, 2016–2024, doi:10.1109/TBME.2017.2676243.
3. Casalino, G.; Castellano, G.; Zaza, G. A MHealth Solution for Contact-Less Self-Monitoring of Blood Oxygen Saturation. In Proceedings of the 2020 IEEE Symposium on Computers and Communications (ISCC), Rennes, France, 7–10 July 2020; pp. 1–7.
4. Athaya, T.; Choi, S. An Estimation Method of Continuous Non-Invasive Arterial Blood Pressure Waveform Using Photoplethysmography: A U-Net Architecture-Based Approach. *Sensors* **2021**, *21*, 1867, doi:10.3390/s21051867.
5. Shamir, M.; Eidelman, L.A.; Floman, Y.; Kaplan, L.; Pizov, R. Pulse Oximetry Plethysmographic Waveform during Changes in Blood Volume. *Br. J. Anaesth.* **1999**, *82*, 178–181, doi:10.1093/bja/82.2.178.
6. Jindal, G.D.; Ananthakrishnan, T.S.; Jain, R.K.; Sinha, V.; Kini, A.R.; Deshpande, A.K. Non-Invasive Assessment of Blood Glucose by Photo Plethysmography. *IETE J. Res.* **2008**, *54*, 217–222, doi:10.1080/03772063.2008.10876202.
7. Sen Gupta, S.; Kwon, T.-H.; Hossain, S.; Kim, K.-D. Towards Non-Invasive Blood Glucose Measurement Using Machine Learning: An All-Purpose PPG System Design. *Biomed. Signal Process. Control* **2021**, *68*, 102706, doi:10.1016/j.bspc.2021.102706.
8. Alicic, R.Z.; Rooney, M.T.; Tuttle, K.R. Diabetic Kidney Disease. *Clin. J. Am. Soc. Nephrol. CJASN* **2017**, *12*, 2032–2045, doi:10.2215/CJN.11491116.
9. Leon, B.M.; Maddox, T.M. Diabetes and Cardiovascular Disease: Epidemiology, Biological Mechanisms, Treatment Recommendations and Future Research. *World J. Diabetes* **2015**, *6*, 1246–1258, doi:10.4239/wjd.v6.i13.1246.
10. Tan, H.L.; van Dongen, L.H.; Zimmerman, D.S. Sudden Cardiac Death in Young Patients with Diabetes: A Call to Study Additional Causes beyond Ischaemic Heart Disease. *Eur. Heart J.* **2020**, *41*, 2707–2709, doi:10.1093/eurheartj/ehaa011.
11. Jung, D.G.; Jung, D.; Kong, S.H. A Lab-on-a-Chip-Based Non-Invasive Optical Sensor for Measuring Glucose in Saliva. *Sensors* **2017**, *17*, 2607, doi:10.3390/s17112607.

12. Bruen, D.; Delaney, C.; Florea, L.; Diamond, D. Glucose Sensing for Diabetes Monitoring: Recent Developments. *Sensors* **2017**, *17*, 1866, doi:10.3390/s17081866.
13. Yang, D.; Afroosheh, S.; Lee, J.O.; Cho, H.; Kumar, S.; Siddique, R.H.; Narasimhan, V.; Yoon, Y.-Z.; Zayak, A.T.; Choo, H. Glucose Sensing Using Surface-Enhanced Raman-Mode Constraining. *Anal. Chem.* **2018**, *90*, 14269–14278, doi:10.1021/acs.analchem.8b03420.
14. Tang, L.; Chang, S.J.; Chen, C.-J.; Liu, J.-T. Non-Invasive Blood Glucose Monitoring Technology: A Review. *Sensors* **2020**, *20*, 6925, doi:10.3390/s20236925.
15. Zhang, Y.J.; Kwon, H.; Miri, M.-A.; Kallos, E.; Cano-Garcia, H.; Tong, M.S.; Alu, A. Noninvasive Glucose Sensor Based on Parity-Time Symmetry. *Phys. Rev. Appl.* **2019**, *11*, 044049, doi:10.1103/PhysRevApplied.11.044049.
16. Shokrekhodaei, M.; Quinones, S. Review of Non-Invasive Glucose Sensing Techniques: Optical, Electrical and Breath Acetone. *Sensors* **2020**, *20*, 1251, doi:10.3390/s20051251.
17. NGSP: HbA1c and EAG. Available online: http://www.ngsp.org/A1ceAG.asp (accessed on 23 July 2021).
18. Martín-Mateos, P.; Dornuf, F.; Duarte, B.; Hils, B.; Moreno-Oyervides, A.; Bonilla-Manrique, O.E.; Larcher, F.; Krozer, V.; Acedo, P. In-Vivo, Non-Invasive Detection of Hyperglycemic States in Animal Models Using Mm-Wave Spectroscopy. *Sci. Rep.* **2016**, *6*, 34035, doi:10.1038/srep34035.
19. Saraoğlu, H.M.; Selvi, A.O. Determination of Glucose and Hba1c Values in Blood from Human Breath by Using Radial Basis Function Neural Network via Electronic Nose. In Proceedings of the 2014 18th National Biomedical Engineering Meeting, Istanbul, Turkey, 16–17 October 2014; pp. 1–4.
20. Mandal, S.; Manasreh, M.O. An In-Vitro Optical Sensor Designed to Estimate Glycated Hemoglobin Levels. *Sensors* **2018**, *18*, 1084, doi:10.3390/s18041084.
21. Hossain, S.; Gupta, S.S.; Kwon, T.-H.; Kim, K.-D. Derivation and Validation of Gray-Box Models to Estimate Noninvasive In-Vivo Percentage Glycated Hemoglobin Using Digital Volume Pulse Waveform. *Sci. Rep.* **2021**, *11*, 1–18, doi:10.1038/s41598-021-91527-2.
22. Hossain, S.; Kwon, T.H.; Kim, K.D. Estimation of Molar Absorption Coefficients of HbA1c in Near UV-Vis-SW NIR Light Spectrum. *Korean Inst. Commun. Inf. Sci.* **2020**, *46*, 1030–1039.
23. Prahl, S.A. Tabulated Molar Extinction Coefficient for Hemoglobin in Water. Available online: https://omlc.org/spectra/hemoglobin/summary.html (accessed on 1 August 2019).